

Robust moiré flatbands within a broad band-offset range

Peilong Hong^{a,b,d*}, Yi Liang^{c,+}, Zhigang Chen^d, Guoquan Zhang^d

^aSchool of Optoelectronic Science and Engineering, University of Electronic Science and Technology of China (UESTC), Chengdu, Sichuan 611731, China

^bSchool of Mathematics and Physics, Anqing Normal University, Anqing, Anhui 246133, China

^cGuangxi Key Lab for Relativistic Astrophysics, Center on Nanoenergy Research, School of Physical Science and Technology, Guangxi University, Nanning, Guangxi 530004, China

^dThe MOE Key Laboratory of Weak-Light Nonlinear Photonics, School of Physics and TEDA Applied Physics Institute, Nankai University, Tianjin 300457, China

Abstract. Photonic analogs of the moiré superlattices mediated by interlayer electromagnetic coupling are expected to give rise to rich phenomena such as nontrivial flatband topology. Here, we propose and demonstrate a scheme to tune the flatbands in a bilayer moiré superlattice by employing the band offset. The band offset is changed by fixing the bands of one slab while shifting those of the other slab, which is accomplished by modifying the thickness of the latter slab. Our results show that the band-offset tuning not only makes some flatbands emerge and disappear, but also leads to two sets of flatbands that are robustly formed even with the change of band offset over a broad range. These robust flatbands form either at the AA-stack site or at the AB-stack site, and as a result, a single-cell superlattice can support a pair of high-quality localized modes with tunable frequencies. Moreover, we develop a diagrammatic model to provide an intuitive insight into the formation of the robust flatbands. Our work demonstrates a simple yet efficient way to design and control complex moiré flatbands, providing new opportunities to utilize photonic moiré superlattices for advanced light-matter interaction including lasing and nonlinear harmonic generation.

Keywords: moiré superlattice, robust flatbands, doubly-resonant superlattice, diagrammatic model.

* plhong@uestc.edu.cn + liangyi@gxu.edu.cn

1 Introduction

Moiré physics is a nascent yet exciting research direction that has led to important discoveries in various areas, ranging from electronics, to optics, and to acoustics.¹⁻⁴ Moiré physics is associated with the emergence of novel phases that are not present in the individual lattices of the superlattice, leading to intriguing physical phenomena. For instance, when two monolayer materials are brought into contact, the moiré potentials have been predicted and demonstrated to strongly modify the optical properties of the bilayer materials.⁵⁻⁹ Indeed, the initial breakthrough was made in condensed matter systems by discovering exotic phenomena in moiré superlattices, including unconventional superconductivity,¹⁰ moiré excitons,⁶⁻⁹ anomalous Hall ferromagnetism,¹¹ to name just a few. These novel moiré effects are discovered in superlattices with appropriate interlayer coupling, but the realization of the nontrivial superlattice needs fine tuning of the 2d materials, as initiated by the seminal work on twisted bilayer graphene.^{10,12} The difficulty arises from the reliance of the moiré effects on the formation of flatbands that only occur at magic angles in the superlattices.^{10,12,13} Later, the concept of moiré physics was introduced into the realm of optics,

where flexible control on superlattices is feasible.^{2,4} The tunability of photonic superlattices is particularly beneficial for exploring flatband physics and relevant photonic applications.

In photonics, several research groups have studied intriguing moiré physics with mismatched photonic lattices,^{14,15} and twisted bilayer photonic slabs.^{16–20} The moiré bands are typically tuned either by twisting the bilayer slabs or by modifying the optical distance between the two slabs. Especially, the flatbands relevant to novel moiré physics are found at photonic magic angles,^{16,20} demonstrating a striking similarity with the electronic twisted bilayer graphene. Besides, a flatband can also emerge by setting the optical distance to specific values, as discovered in the 2D twisted superlattices^{16,19} and 1D mismatched superlattices.¹⁵ The appearance of flatbands underlies various optical phenomena such as topological transition of optical dispersion contours,¹⁷ non-Anderson-type localization of light,²¹ twisting-induced optical solitons,²² and moiré quasi-bound states in the continuum.²³ Obviously, flatbands play an essential role in exploring novel physics in optics. Besides, a flatband mode is typically localized,^{24,25} making it highly valuable for manipulating light-matter interaction such as lasing²⁶ and optical harmonic generation.²⁷ Therefore, flatband formation lies at the heart of intriguing moiré physics and relevant applications. It is desirable and critical to develop efficient strategies to tune the moiré flatbands.

In this work, we employ the band offset in the band domain as an efficient knob to tune the flatbands in a mismatched bilayer superlattice. The band offset is changed by fixing the bands of one slab while shifting those of the other slab, which are realizable by modifying the thickness of the latter slab in practice. Remarkably, the band offset not only triggers the appearance and disappearance of a few flatbands, but also leads to two sets of flatbands that can robustly form within a broad band-offset range. By taking advantage of the robustly formed flatbands, we further demonstrate a doubly-resonant single-cell superlattice with localized modes originating from the flatbands, and the frequencies of these modes are tunable by band offset. Such localized modes hold great promise for manipulating advanced light-matter interaction. Moreover, we develop a diagrammatic model to provide an intuitive insight into the formation of these robust flatbands, which can inspire new design approaches for moiré superlattices with tailored flatbands. Our work thus provides an efficient way to understand and control the formation of flatbands. Since the robust flatbands can be achieved without requiring strict magic configuration, they may have great potential in relevant applications based on moiré devices.

2 Results

2.1 Scheme and adjustable band offset

Our superlattice is constructed by stacking two mismatched silicon slabs in a commensurate configuration shown in Figure 1(a). The unit size of slab 1 is $a_1 = 2N/(2N + 1)a_0$, while that of slab 2 is $a_2 = 2(N + 1)/(2N + 1)a_0$. Here, N is an integer (fixed to be 13 hereafter), and $a_0 = 300$ nm. The resulting moiré superlattice has a unit size $a_M = (N + 1)a_1 = Na_2$. Certainly, one can

choose other values of N , and a_M changes accordingly. The width of the silicon strip is fixed to be $w_i = 0.7a_i$ ($i = 1, 2$). In the superlattice, slab-1's silicon strip can align with slab-2's silicon strip, creating the AA-stack site, indicated as "A" in Figure 1(a). Slab-1's silicon strip can also align with the slab-2's air gap, creating the AB-stack site, indicated as "B" in Figure 1(a).

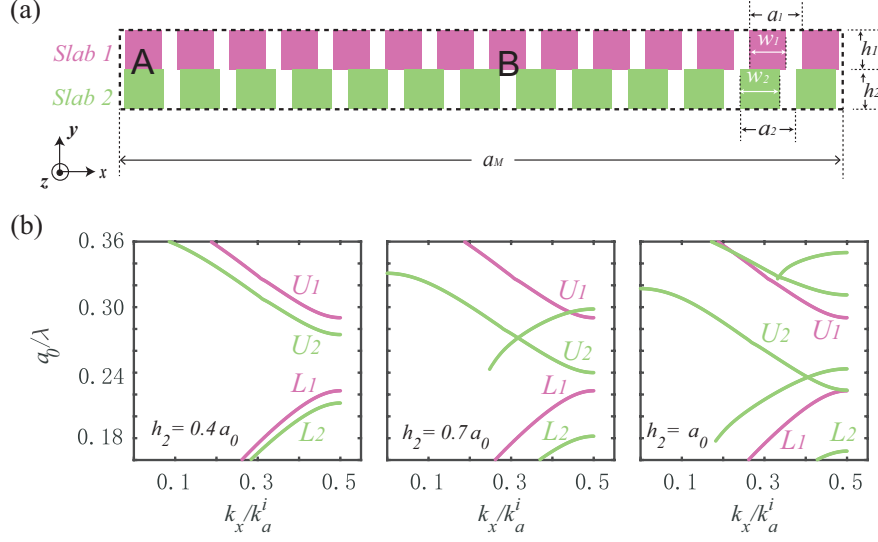


Fig 1 (a) Schematic diagram of a silicon moiré superlattice. (b) band offset adjusted by the thickness (h_2) of slab 2. Here, the bands are calculated only for single slab, in the absence of the other slab. $k_a^i = 2\pi/a_i$ ($i = 1, 2$). Note that more than two bands for slab 2 emerge within the interested region by adjusting h_2 , but only two main bands L_i and U_i are marked.

To exploit the band offset as a degree of freedom to tune the moiré bands in the superlattice, we keep the thickness (h_1) of slab 1 fixed at $0.4a_0$, but change the thickness (h_2) of slab 2 from $0.4a_0$ to a_0 . As a result, the bands of slab 1 remain unchanged, while the spectral positions of slab-2's bands are shifted. Hence, the band offset between the two slabs is modified. Hereafter, we focus on the TE bands, of which the electric field is polarized along z axis. The TE bands at different conditions are obtained by solving the wave equation

$$\nabla \times (\nabla \times \mathbf{E}_z) - \frac{\omega^2}{c_0^2} \epsilon_r \mathbf{E}_z = 0. \quad (1)$$

Here, ω is the frequency, c_0 is the velocity of light in the vacuum, and ϵ_r is the relative permittivity. The refractive indices of the silicon and the air are set to be 3.47 and 1, respectively. In this work, the wave equation is numerically solved through finite-element computation with Comsol Multiphysics. Notably, some bands of the photonic slabs are above the light line $\omega = c_0 k_x$, and therefore light can leak into the free space surrounding the slabs. Consequently, the eigenfrequency is typically a complex value $\omega_r + i\gamma$, and the quality factor $Q = \omega_r/(2\gamma)$ describes how well an eigenmode is confined in the slabs.

Figure 1(b) shows the TE bands of the two slabs at different h_2 ($= 0.4a_0, 0.7a_0, a_0$). For

clarity, we only draw the eigenmodes with quality factors $Q > 50$, and therefore some bands look incomplete in the figure. Within the spectral range of interest, slab 1 has two lowest bands (L_1 and U_1) that remain unchanged in the band domain. Slab 2 also has two lowest bands (L_2 and U_2) at $h_2 = 0.4a_0$, and an initial band offset between L_1 and L_2 (U_1 and U_2) can be seen. When h_2 increases to $0.7a_0$, L_2 and U_2 move downward, while U_2 intersects with another band. As h_2 increases to a_0 , L_2 and U_2 move downward further. Clearly, the band offset between L_1 and L_2 (U_1 and U_2) increases with the increase of the thickness h_2 . Thus, the band offset is adjusted efficiently by scanning the thickness h_2 of slab 2.

2.2 Robust flatbands

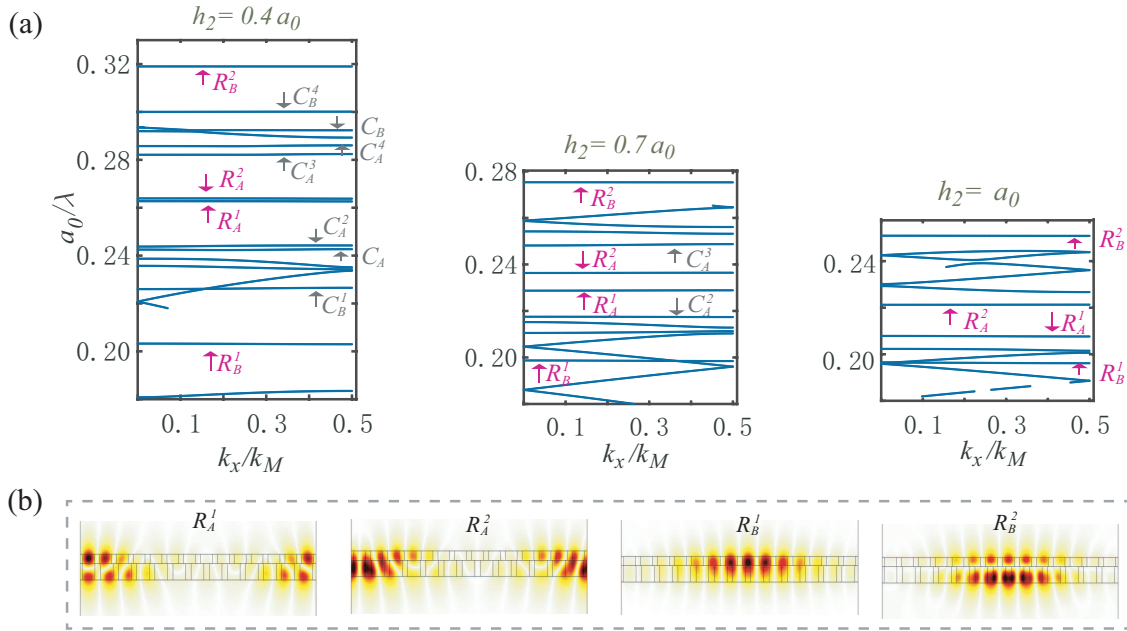


Fig 2 (a) Moiré bands at different band offsets. The flatbands are marked by different symbols, where C labels the conventional flatbands that come and go by band-offset tuning, R labels the robust flatbands that preserve. The subscript A (or B) such as in R_A^1 denotes the center of field pattern at A (or B) site, and the superscript $i = 1, 2, \dots$ denotes different flatbands. Here, $k_M = 2\pi/a_M$, and a same symbol at different h_2 indicates that the eigenmodes have similar field patterns. (b) The field patterns $|E_{eigen}(k_x = 0)|$ of the four robust flatbands R_A^1, R_A^2, R_B^1 and R_B^2 in a single cell of a periodic superlattice at $h_2 = 0.7a_0$. The field magnitude is represented by a reversed hot colormap with the maximum in black and the minimum in white.

Next, we investigate how the moiré bands are tuned by the band offset. The moiré bands of the superlattice (with $h_2 = 0.4a_0, 0.7a_0$ and a_0) are shown in Figure 2(a). The cell length a_M of the superlattice is much larger, i.e. N times of that of slab 2. As a result, while a band of slab 2 can extend over $2\pi/a_2$ in the k -space, the superlattice has mini-bands that only extend over $1/N$ of $2\pi/a_2$ in the k -space. We have identified the flatbands that have a frequency deviation meeting the condition $(f_{max} - f_{min})/(f_{max} + f_{min}) < 0.15\%$. For clarity, the flatbands with similar field

patterns are marked by a same symbol. The results show that multiple flatbands emerge at each band offset, but some flatbands may disappear when the band offset changes. Specifically, the flatbands $C_A^1, C_A^4, C_B^1, C_B^3$ and C_B^4 emerge at $h_2 = 0.4a_0$, but disappear at $h_2 = 0.7a_0$ and a_0 . The flatband C_A^2 has a frequency deviation of 0.08% at $h_2 = 0.4a_0$ and a smaller frequency deviation of 0.02% at $h_2 = 0.7a_0$, but disappears at $h_2 = a_0$. The flatband C_A^3 has a frequency deviation of 0.05% and a larger frequency deviation of 0.12% at $h_2 = 0.7a_0$, but disappears at $h_2 = a_0$. Such emerging and disappearing flatbands demonstrate the important role of band offset in tuning the flatbands.

Remarkably, there are four flatbands that can form robustly at different band offsets through the entire scan range, labeled as R_A^1, R_A^2, R_B^1 and R_B^2 in Figure 2(a) for clarity. The field patterns of these robust flatbands are shown in Figure 2(b). It is seen that the R_A^1 and R_A^2 modes are strongly localized around A site of the superlattice, while the R_B^1 and R_B^2 modes are strongly localized around B site of the superlattice. The stable formation of the flatbands is quite desirable in practice, because they can be achieved without the need for a subtle magic configuration.

2.3 Doubly-resonant single-cell superlattice

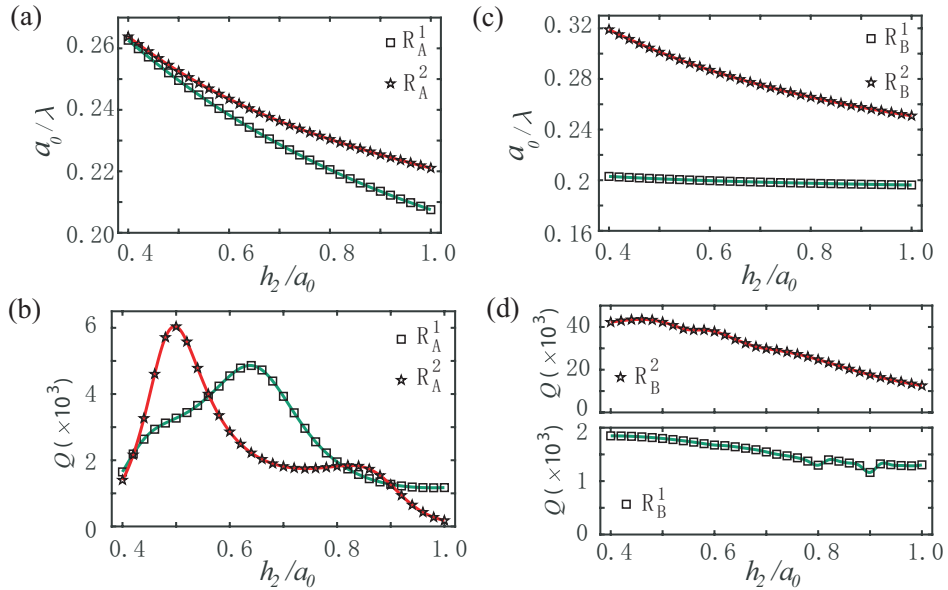


Fig 3 Tunable spectral positions of the R_A^1 and R_A^2 modes (a) and that of the R_B^1 and R_B^2 modes (c). The quality factors of the R_A^1 and R_A^2 modes (b) and that of the R_B^1 and R_B^2 modes (d) hold high values.

The simultaneous emergence of multiple robust flatbands paves the way toward multiply-resonant superlattice with tunable frequencies, since scanning the band offset does not make these flatbands disappear but rather allows us to control their spectral positions. Particularly, these robust flatbands can even be supported by only a single-cell superlattice, due to their strongly localized

wavefunctions. We thus calculate the eigenfrequencies of localized modes with a single-cell superlattice, and focus on those originating from the robust flatbands. The R_A^1 and R_A^2 modes are studied with an A-site centered single-cell superlattice, while R_B^1 and R_B^2 modes are studied with a B-site centered single-cell superlattice. The spectral positions of R_A^1 and R_A^2 modes at different h_2 are shown in Figure 3(a), and those for R_B^1 and R_B^2 modes are shown in Figure 3(c). The R_A^1 and R_A^2 modes are nearly degenerate at $0.4a_0$, and gradually separate when h_2 increases. In contrast, R_B^1 and R_B^2 modes start at a large spectral separation, and become closer in spectrum when h_2 increases. Notably, the frequency of R_B^1 mode keeps almost invariant against the change of h_2 .

Besides, we calculated the quality factor of these flatband modes at different h_2 . The quality factor of R_A^1 mode is peaked at $h_2 = 0.64a_0$ with a value ~ 5000 , but keeps larger than 1000 within the entire range as shown in Figure 3(b). The quality factor of R_A^2 mode is peaked near $h_2 = 0.5a_0$ with a value ~ 6000 , but keeps larger than 1000 up to $h_2 = 0.9a_0$. For R_B^1 and R_B^2 modes shown in Figure 3(d), the quality factor of R_B^1 mode decreases slightly from ~ 2000 to ~ 1300 within the scan range, while the quality factor of R_B^2 mode keeps a high value that is between ~ 12000 and ~ 43000 . These results show that the robust-flatband resonances hold high quality even in a single-cell superlattice, demonstrating the possibility of constructing a high-quality multiply-resonant superlattice.

2.4 A diagrammatic model

Next, we provide an intuitive insight into the formation of the robust flatbands by employing a simplified two-site coupled-band diagram. Our model originates from the realization that the local dielectric structure continuously changes from A site to B site in the superlattice, i.e. other local positions in the superlattice have effective dielectric structures belonging to the intermediate states between A site and B site. Consequently, we consider a two-site diagram that only consists of two sets of bands related to A site and B site. Specifically, one set of bands corresponds to a fictitious lattice with an A-site-like unit cell, and the other set of bands corresponds to a fictitious lattice with B-site-like unit cell. The bands of the fictitious lattices originate from the interlayer coupling between the two slabs. Under a two-mode coupling approximation, the eigenfrequencies of coupled eigenmodes are given by²⁸

$$\omega_{\pm}^c = \frac{\omega_1 + \omega_2}{2} \pm \sqrt{\mu^2 + \left(\frac{\omega_1 - \omega_2}{2}\right)^2}. \quad (2)$$

Here $\omega_i (i = 1, 2)$ denotes the frequency of the eigenmode of slab i such as L_i/U_i schematically shown in Figure 4(a), and ω_{\pm}^c denotes the frequencies of the coupled eigenmodes. Generally, a strong interlayer coupling coefficient μ leads to a larger spectral gap between the pair of coupled eigenmodes compared to $|\omega_1 - \omega_2|$. The interlayer coupling coefficient μ is determined by the overlap of the field patterns that correspond to the pair of eigenmodes $\omega_i (i = 1, 2)$.²⁹ Specifically,

$L_i (i = 1, 2)$ has a spot-like field pattern with its maxima at the silicon strip, while $U_i (i = 1, 2)$ has a spot-like field pattern with its maxima at the air gap. At the A site, the field maxima of L_1 (U_1) align with that of L_2 (U_2), such that their coupling coefficient μ is large. The strong coupling increases the spectral gap between L_1 and L_2 (U_1 and U_2), forming a coupled band diagram schematically shown in Figure 4(b). At the B site, the field maxima of L_1 align with that of U_2 , and thus their coupling coefficient μ is large. The strong coupling increases the spectral gap between L_1 and U_2 , leading to a bandgap structure schematically shown in Figure 4(c). The two sets of coupled bands in Figure 4(b) and 4(c) constitute our two-site coupled-band diagram.

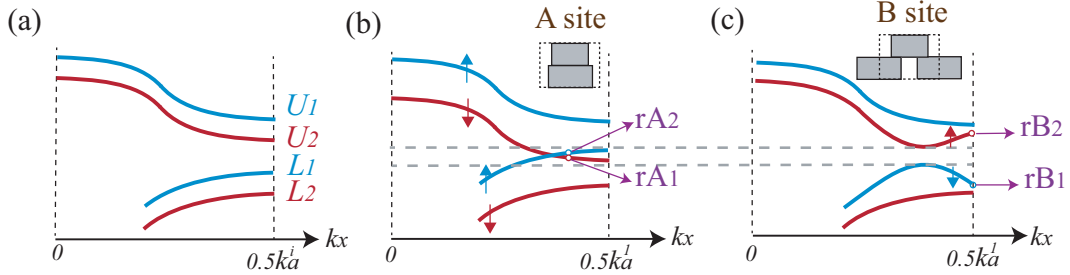


Fig 4 Two-site coupled-band diagram. (a) The band map represents the lowest two bands L_i and U_i ($i = 1, 2$) of individual slabs of the moiré superlattice. (b) The band structure for an A-site like fictitious lattice. The interlayer coupling between L_1 and L_2 (U_1 and U_2) is maximized (as indicated by the arrows). (c) The band map of a B-site like fictitious lattice. The interlayer coupling between L_1 and U_2 is maximized.

In this simplified two-site band diagram, two bands (rA_1 and rA_2) at A site always locate within the bandgap at B site. This unique band structure gives rise to optical modes that are hosted at A site but do not extend to B site. Consequently, a pair of robust flatbands always form at A site, as long as the coupled-band gap structure does not change. This explains the robust formation of the flatbands R_A^1 and R_A^2 at A site in the superlattice. On the other hand, the pair of coupled bands at B site (rB_1 and rB_2) reach extrema at the band edges, which are related to the robust flatbands R_B^1 and R_B^2 . Although the coupled-band edges do not locate within a bandgap at A site, they are in resonance with only one band point at A site. Moreover, the strong band coupling makes the spatial patterns of coupled eigenmodes at B site poorly overlap with those of the resonant eigenmodes at A site. As a result, the leakage to A site is weak, leading to the formation of R_B^1 and R_B^2 localized at B site. The flatbands R_B^1 and R_B^2 are stable as long as the coupled-band structure persists. Thus, the simple two-site band diagram gives us an intuitive understanding of the formation of the robust flatbands.

To further confirm the diagrammatic model, we implement full-wave calculation to obtain the accurate coupled bands of the A-site and B-site like fictitious lattices, separately. Figures 5(a)-5(c) show the two-site coupled bands at different h_2 ($= 0.4a_0, 0.7a_0$ and a_0). The crossing bands at A site, as well as the band gap at B site, are clearly seen in the results. Moreover, we draw the field patterns of the four modes marked by A_1 , A_2 , B_1 and B_2 in Figure 5(b), as seen in Figure 5(d).

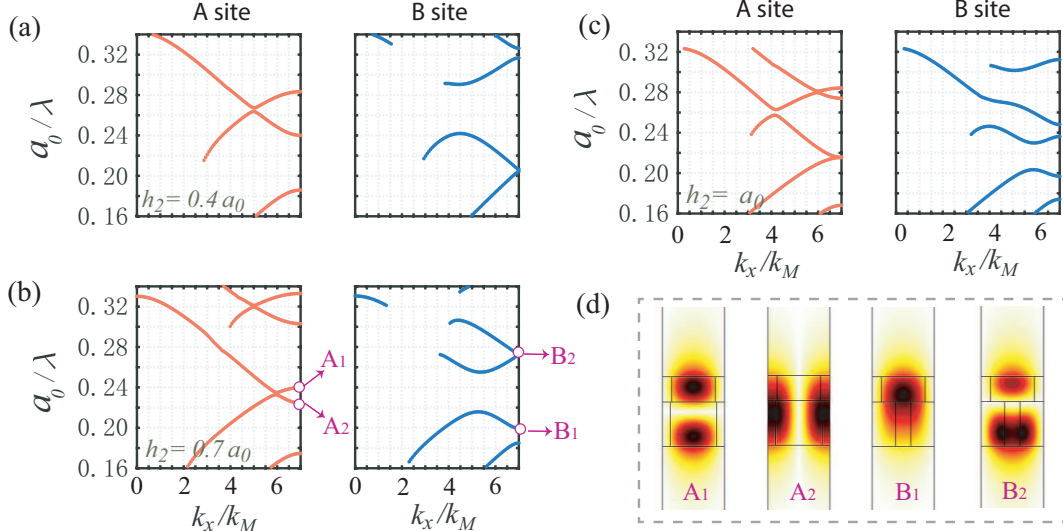


Fig 5 Coupled bands for the A-site like and B-site like fictitious lattices at $h_2 = 0.4a_0$ (a), $0.7a_0$ (b), and a_0 (c). The field patterns (d) for the four different band-edge modes as indicated by A_1 , A_2 , B_1 and B_2 in (b). Again, the field magnitude is represented by a reversed hot colormap.

These field patterns are in a good agreement with the field patterns of the robust flatbands at A site (R_A^1 and R_A^2) and B site (R_B^1 and R_B^2) shown in Figure 2(b). This agreement adequately confirms our theoretical explanation on the formation of the robust flatbands.

3 Discussion

The robust flatbands differ significantly from those that are sensitive to the change of band offset, indicating the complex formation process of moiré flatbands. The proposed diagrammatic model provides an intuitive understanding on the formation of robust flatbands with regard to the band offset. Notably, the situation in twisted superlattices is much more complicated than the global band offset simply used in our work. When the twist angle is adjusted, locally variable band offsets are introduced in the parameter space, together with twist-dependent dielectric structures in the real space. Nonetheless, our results may provide a straightforward approach for comprehending the formation of relatively stable flatbands in twisted superlattices.^{30,31}

Besides, the diagrammatic model can guide new designs of moiré superlattices. For instance, one can intentionally design two unit cells, and let them form a two-site band diagram similar to that shown in Figures 4(b) and 4(c). The two unit cells can be bilayer ones, as well as multi-layer ones or even monolayer ones. Then, a moiré superlattice can be constructed by connecting the two unit cells with intermediate-state cells, of which the formation of robust flatbands can be predicted under the two-site band diagram. The field patterns of the robust flatbands can also be estimated by referring to the eigenmodes of the pair of unit cells. Clearly, our two-site diagrammatic model significantly simplifies the design of moiré superlattices with tailored flatbands.

Furthermore, due to the robust formation of these flatband modes, it is possible to achieve dynamic control of their frequencies in practice. For instance, one can fabricate a lattice with multiple domains, and each domain has a different thickness. By shifting the multiple-domain lattice with regard to another finite-size lattice of fixed thickness, the flatband modes stably form in the bilayer region, but alter their frequencies. Therefore, the band-offset tuning has great potential for enhancing functionalities of moiré photonic devices. Certainly, structural perturbations in the superlattice could affect the flatbands, with the extent of this influence dependent on the specific fabrication conditions. Further studies are necessary to explore and understand these effects, which may be useful for experimental implementations, especially as several experimental techniques have demonstrated their capability of realizing nontrivial moiré superlattices, including nanofabrication,²⁶ photorefractive effect,^{21,22} and femtosecond-laser writing.³²

4 Conclusion

In conclusion, we have demonstrated that the band offset can be an efficient knob to tune the flatbands in a moiré superlattice. The band offset not only makes a few flatbands emerge and disappear, but also leads to multiple robust flatbands with their wavefunctions localized at different stacking sites. These robust flatbands offer promising avenues for constructing multiply-resonant moiré superlattices with tunable frequencies, as illustrated by the analysis of a single-cell superlattice. Moreover, we have developed a diagrammatic model that provides an intuitive insight into the formation mechanism of the two sets of robust flatbands, which can inspire new designs of moiré superlattices. Our scheme may be further developed with AI-empowered techniques, which may prove relevant to next-generation device designs for nanophotonics.³³ In particular, this work represents an important step toward controlling and understanding complex flatbands in moiré superlattices, and may bring about new opportunities for exploiting moiré superlattices in manipulating advanced light-matter interactions such as lasing,²⁶ nonlinear harmonic generation,²⁷ and enhanced free-electron radiation.³⁴

Disclosures

The authors declare no conflict of interest.

Acknowledgments

This work was supported by Sichuan Science and Technology Program (2023NSFSC0460), the Fundamental Research Funds for the Central Universities (ZYGX2020J010), the Open Project Funding of the Ministry of Education Key Laboratory of Weak-Light Nonlinear Photonics (OS22-1), Guangxi Natural Science Foundation (2020GXNSFAA297041), the National Key R&D Program of China (2022YFA1404800), and the National Natural Science Foundation (12134006).

Data Availability

The data that support the findings of this article are not publicly available. They can be requested from the corresponding authors upon reasonable request.

References

- 1 E. Y. Andrei, D. K. Efetov, P. Jarillo-Herrero, *et al.*, “The marvels of moiré materials,” *Nat. Rev. Mater.* **6**(3), 201–206 (2021).
- 2 J. Chen, X. Lin, M. Chen, *et al.*, “A perspective of twisted photonic structures,” *Appl. Phys. Lett.* **119**(24), 240501 (2021).
- 3 Y. Deng, M. Oudich, N. J. Gerard, *et al.*, “Magic-angle bilayer phononic graphene,” *Phys. Rev. B* **102**(18), 180304(R) (2020).
- 4 L. Du, M. R. Molas, Z. Huang, *et al.*, “Moiré photonics and optoelectronics,” *Science* **379**(6639), eadg0014 (2023).
- 5 B. Urbaszek and A. Srivastava, “Materials in flatland twist and shine,” *Nature* **567**, 30–40 (2019).
- 6 K. Tran, G. Moody, F. Wu, *et al.*, “Evidence for moiré excitons in van der waals heterostructures,” *Nature* **567**(7746), 71–75 (2019).
- 7 K. L. Seyler, P. Rivera, H. Yu, *et al.*, “Signatures of moiré-trapped valley excitons in mose2/wse2 heterobilayers,” *Nature* **567**(7746), 66–70 (2019).
- 8 E. M. Alexeev, D. A. Ruiz-Tijerina, M. Danovich, *et al.*, “Resonantly hybridized excitons in moiré superlattices in van der waals heterostructures,” *Nature* **567**(7746), 81–86 (2019).
- 9 C. Jin, E. C. Regan, A. Yan, *et al.*, “Observation of moiré excitons in wse₂/ws₂ heterostructure superlattices,” *Nature* **567**(7746), 76–80 (2019).
- 10 Y. Cao, V. Fatemi, S. Fang, *et al.*, “Unconventional superconductivity in magic-angle graphene superlattices,” *Nature* **556**(7699), 43–50 (2018).
- 11 N. Bultinck, S. Chatterjee, and M. P. Zaletel, “Mechanism for anomalous hall ferromagnetism in twisted bilayer graphene,” *Phys. Rev. Lett.* **124**(16), 166601 (2020).
- 12 Y. Cao, V. Fatemi, A. Demir, *et al.*, “Correlated insulator behaviour at half-filling in magic-angle graphene superlattices,” *Nature* **556**(7699), 80–84 (2018).
- 13 R. Bistritzer and A. H. MacDonald, “Moiré bands in twisted double-layer graphene,” *Proc. Natl. Acad. Sci. U. S. A.* **108**(30), 12233–12237 (2011).
- 14 W. Wang, W. Gao, X. Chen, *et al.*, “Moiré fringe induced gauge field in photonics,” *Phys. Rev. Lett.* **125**(20), 203901 (2020).
- 15 D. X. Nguyen, X. Letartre, E. Drouard, *et al.*, “Magic configurations in moiré superlattice of bilayer photonic crystals: Almost-perfect flatbands and unconventional localization,” *Phys. Rev. Res.* **4**(3), L032031 (2022).

- 16 K. Dong, T. Zhang, J. Li, *et al.*, “Flat bands in magic-angle bilayer photonic crystals at small twists,” *Phys. Rev. Lett.* **126**(22), 223601 (2021).
- 17 G. Hu, Q. Ou, G. Si, *et al.*, “Topological polaritons and photonic magic angles in twisted α -moo3 bilayers,” *Nature* **582**(7811), 209–213 (2020).
- 18 B. Lou, N. Zhao, M. Minkov, *et al.*, “Theory for twisted bilayer photonic crystal slabs,” *Phys. Rev. Lett.* **126**(13), 136101 (2021).
- 19 M. Oudich, G. Su, Y. Deng, *et al.*, “Photonic analog of bilayer graphene,” *Phys. Rev. B* **103**(21), 214311 (2021).
- 20 H. Tang, F. Du, S. Carr, *et al.*, “Modeling the optical properties of twisted bilayer photonic crystals,” *Light Sci. Appl.* **10**(1), 1–8 (2021).
- 21 P. Wang, Y. Zheng, X. Chen, *et al.*, “Localization and delocalization of light in photonic moiré lattices,” *Nature* **577**(7788), 42–46 (2020).
- 22 Q. Fu, P. Wang, C. Huang, *et al.*, “Optical soliton formation controlled by angle twisting in photonic moiré lattices,” *Nat. Photonics* **14**(11), 663–668 (2020).
- 23 L. Huang, W. Zhang, and X. Zhang, “Moiré quasibound states in the continuum,” *Phys. Rev. Lett.* **128**(25), 253901 (2022).
- 24 D. Leykam, A. Andreanov, and S. Flach, “Artificial flat band systems: from lattice models to experiments,” *Adv. Phys.: X* **3**(1), 1473052 (2018).
- 25 L. Tang, D. Song, S. Xia, *et al.*, “Photonic flat-band lattices and unconventional light localization,” *Nanophotonics* **9**(5), 1161–1176 (2020).
- 26 X.-R. Mao, Z.-K. Shao, H.-Y. Luan, *et al.*, “Magic-angle lasers in nanostructured moiré superlattice,” *Nat. Nanotechnol.* **16**(10), 1099–1105 (2021).
- 27 P. Hong, L. Xu, C. Ying, *et al.*, “Flatband mode in photonic moiré superlattice for boosting second-harmonic generation with monolayer van der waals crystals,” *Opt. Lett.* **47**(9), 2326–2329 (2022).
- 28 M.-A. Miri and A. Alù, “Exceptional points in optics and photonics,” *Science* **363**(6422), eaar7709 (2019).
- 29 H. A. Haus and W. Huang, “Coupled-mode theory,” *Proc. IEEE* **79**(10), 1505–1518 (1991).
- 30 H. Wang, S. Ma, S. Zhang, *et al.*, “Intrinsic superflat bands in general twisted bilayer systems,” *Light Sci. Appl.* **11**(1), 159 (2022).
- 31 C.-H. Yi, H. C. Park, and M. J. Park, “Strong interlayer coupling and stable topological flat bands in twisted bilayer photonic moiré superlattices,” *Light Sci. Appl.* **11**(1), 289 (2022).
- 32 A. Arkhipova, Y. Kartashov, S. Ivanov, *et al.*, “Observation of linear and nonlinear light localization at the edges of moiré lattices,” *Phys. Rev. Lett.* **130**(8), 083801 (2023).
- 33 Z. Chen and M. Segev, “Highlighting photonics: looking into the next decade,” *eLight* **1**(1), 2 (2021).

- 34 Y. Yang, C. Roques-Carmes, S. E. Kooi, *et al.*, “Photonic flatband resonances for free-electron radiation,” *Nature* **613**(7942), 42–47 (2023).

Biographies and photographs of the authors are not available now.